International Symposium
On Turbulence and Shear Flow
Phenomena (TSFP-9)
June 30 - July 3, 2015 *Melbourne, Australia*

IMPLICIT LARGE EDDY SIMULATION OF PREMIXED TURBULENT COMBUSTION WITH MULTI-SCALE ENERGY INJECTION

Song Zhao
ICARE-CNRS
1c, avenue de la Recherche Scientifique,
F-45071 Orléans cedex2, France
song.zhao@cnrs-orleans.fr

Nicolas Lardjane
CEA, DAM, DIF
F-91297 Arpajon, France
nicolas.lardjane@cea.fr

Ivan Fedioun
ICARE-CNRS
1c, avenue de la Recherche Scientifique,
F-45071 Orléans cedex2, France
ivan.fedioun@cnrs-orleans.fr

ABSTRACT

An experimental Bunsen burner with multi-grid turbulent forcing is simulated with a compressible solver based on different WENO schemes. Their built-in numerical dissipation allow different (I)LES strategies: the flow subgrid scales are always implicitly modeled by numerics, but the premixed turbulent Methane-air flame is modeled either implicitly, or explicitly by the Thickened Flame Model supplemented by a new model for the subgrid scale wrinkling factor. Results show that a low-dissipation WENO scheme associated with the explicit subgrid combustion model predicts very well the experimental flame length. Pure ILES with advanced WENO schemes produces a slightly shorter but realistic flame, provided the grid spacing is of order of the laminar flame thickness.

CONTEXT OF THE STUDY

The framework of this study is the production of clean energy from gas turbines burning syngas, a mixture of CO and H_2 not always well characterized since it may come from biomass, coal gasification or various organic wastes. If the diversity of the raw material is very attractive for these technologies, the uncertainty on the gas composition is a challenging problem for complete, efficient and safe combustion. One way to optimize the premixed combustion of syngas is to improve the flame/turbulence interactions, i.e. the flame surface density. To that end, one can increase the turbulence intensity of the premixed jet as shown by Yuen & Gülder (2013), but simple grids hardly allow for more than 3∼4% of turbulence intensity. A previous experimental study by Mazellier *et al.* (2010) has shown, in the non-reacting case, that a system of shifted grids with different hole sizes and blockage ratios was able to generate a homogeneous and isotropic turbulence with intensity as high as 15%. This has led to design an experimental Bunsen burner sketched in figure 1, at laboratory ICARE, France.

The burner exit is shown in figure 2. Its inner diameter is $D = 25$ mm and the bulk velocity is $U_D = 3.5$ m/s. A pilot flame is used to stabilize the conical turbulent premixed flame. The jet exits into a vessel which can be pressurized from 0.1 to 1 MPa, matching gas turbine combustion chambers conditions. A thorough experimental investiga-

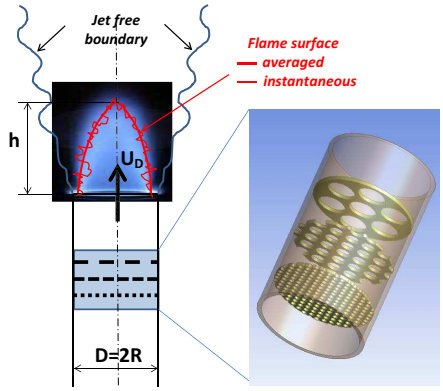

Figure 1. Schematic of the turbulent Bunsen burner with multi-scale forcing.

Figure 2. View of the burner exit with the pilot flame annulus (left), taken from one optical access of the pressurized vessel (right).

tion of the non-reacting flow by Fragner *et al.* (2015*b*) has demonstrated the multi-scale forcing effects on the Taylor microscale (decrease by about 20%) and the spectral distribution of energy (shifted toward the small scales, ratio up to 1.7 in the dissipative range), compared to a single grid turbulence generator. Preliminary observations in the reacting CH_4/air case have shown a deep modification of the flame wrinkling, hence of the turbulent flame speed by this turbulence generator.

The aim of the present study is to simulate numerically this experiment. This challenging task is useful (i) to set up a methodology for complex turbulent inlet conditions, (ii) to confirm/supplement experimental data, (iii) to assess the ability of different implicit large eddy simulation (ILES) strategies to model premixed combustion.

METHODOLOGY

Overview

The ILES procedure is based on 5th order finite difference WENO schemes to solve the hyperbolic (Euler) part of Navier-Stokes equations for 3D, compressible, multi-species reacting flows. Different weighting strategies are implemented: optimum linear weight (OPT), "classical" Jiang & Shu (1996) weights (JS), "mapped" (M) weights by Henrick *et al.* (2005), "improved" (Z) weights by Borges *et al.* (2008) (Z), and (MZ) their combination. The 5th order WENO-JS scheme has been successfully applied to the ILES of transonic non-reacting and supersonic reacting air/H_2 jets by Karaca *et al.* (2012). WENO-M, -Z and -MZ have been evaluated by Zhao *et al.* (2014) on the same test cases, showing no clear advantage of WENO-M and WENO-Z over the classical WENO-JS scheme for this high-speed flow governed by the dynamics of large scale structures. However, the 5th order WENO-MZ scheme has spectral characteristics close to WENO-JS at 7th order, which is a desirable feature for low-speed flows. In this study, a low-Mach formulation based on the artificial acoustic stiffness reduction (ASR) of Wang & Trouvé (2004) is used, reducing the speed of sound by a factor $\alpha \approx 10$, $c \rightarrow c/\alpha$, which allows larger CFL-based time-steps. Time stepping is achieved with a 3rd order Runge-Kutta TVD scheme. Thermodynamics is taken from Burcat & Ruscic (2006). Viscous terms are discretized with 4th order central finite difference. Transport properties are computed with the EGLIB library (Ern & Giovangigli (1996)). Chemistry is implemented as Arrhenius laws in CHEMKIN format.

Multi-scale turbulent inlet

The detailed, full, numerical simulation of the flow through the multiple grids shown in figure 1 is out of reach and not necessary. The idea is to start from an experimental 1D frequency spectrum measured at the outlet of the turbulence generator. A block of "synthetic" HIT showing the same spectral characteristics is generated, and injected at the inlet of the computational domain, as shown in figure 3, using the low-Mach formulation of the characteristic boundary conditions of Thompson (1990).

More precisely, given the time correlation $Q_{11}(\tau) = < u_1'(\vec{x},t)u_1'(\vec{x},t+\tau) >$ at a point $\vec{x}$ (e.g. on the axis) for the sampling frequency $\omega = 2\pi f = 2\pi/\tau$, Taylor's hypothesis gives the space correlation $Q_{11}(\xi) = < u_1'(\vec{x},t)u_1'(\vec{x}+\xi\vec{e_1},t) >$ for the separation $\vec{\xi} = \xi\vec{e_1}$ by setting $\xi = U_1\tau$, i.e. $\omega = U_1 K_1$, where $U_1(\vec{x})$ is the time-mean local longitudinal velocity component and $\vec{e_1}$ the unit vector in the mean flow direction. By varying the sampling frequency, one gets the 1D spatial spectrum $F_{11}(K_1)$ at wavenumber K_1 by FFT. Then, the 3D energy spectrum $E(K)$, defined by $k = \frac{1}{2} < u_i' u_i' > = \int_0^\infty E(K)dK$, is obtained from the HIT relation (Hinze (1975)):

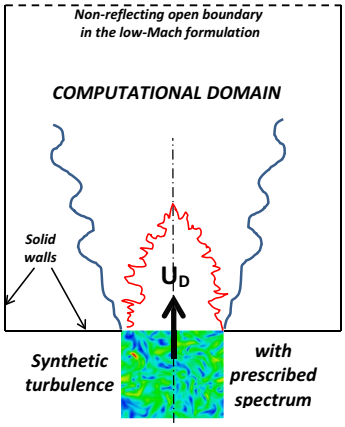

Figure 3. Sketch of the ILES setup.

$$E(K) = K^3 \frac{d}{dK}\left(\frac{1}{K}\frac{dF_{11}(K)}{dK}\right) \qquad (1)$$

Figure 4 shows the raw experimental 1D spectrum and the 3D energy spectrum obtained from (1). Given the energy spectrum, a 3D divergence free random velocity field is generated as described in Fedioun *et al.* (2001). This initial field is advanced for a few turnover times in a DNS pseudo-spectral solver, in order to recover a physical solution of the Navier-Stokes equations. A "cube" of HIT is then generated, that matches the spectral characteristics of the multi-scale experimental forcing.

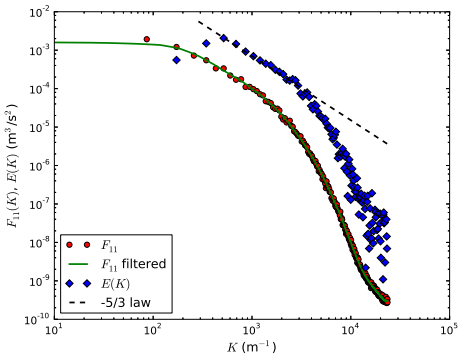

Figure 4. 1D experimental spectrum $F_{11}(K_1)$ and 3D energy spectrum $E(K)$ obtained from (1) after filtering.

Subgrid-scale premixed combustion model

While, as shown by Zhao *et al.* (2014), flow subgrid (sgs) and subfilter (sfs) scales can be implicitly modeled by the built-in filter and dissipative properties of WENO schemes, the flame front of (thermal) thickness $\delta_L^0 = (T_b - T_u)/\max|\nabla T|$ is generally too thin to be resolved on a LES grid and has to be artificially thickened by a factor F. The

loss in resolved flame surface is modeled by the wrinkling factor $\Xi = S_T/S_L^0$ (Colin *et al.* (2000)) where S_T and S_L^0 are the turbulent and laminar flame speeds, respectively. In the (flow) ILES formalism, the Favre-filtered species equation reads

$$\frac{\partial \overline{\rho}\widetilde{Y_\alpha}}{\partial t} + \left(\overline{\rho}\widetilde{u_j}\widetilde{Y_\alpha}\right)_{,j} = -\left(F\Xi\overline{\rho}\widetilde{V_{\alpha j}^c}\widetilde{Y_\alpha}\right)_{,j} + \frac{\Xi}{F}\hat{\dot{\omega}}_\alpha \quad (2)$$

where $\hat{\dot{\omega}}_\alpha = \dot{\omega}_\alpha(\widetilde{Y_\alpha}, \widetilde{T})$ is the chemical source term in quasi-laminar formulation, i.e. computed with resolved variables. Many models for Ξ have been proposed in the literature, either static (Charlette *et al.* (2002)) or dynamic (Wang *et al.* (2011)). In the present study, a new (unpublished yet) sgs model proposed by Thiesset *et al.* (2015) is implemented. This model, derived from Charlette *et al.* (2002), has the form

$$\Xi = \frac{S_T}{S_L^0} = \left\{\left[1+\left(\frac{\Delta_F}{\eta_i}\right)^\alpha\right] / \left[1+\left(\frac{\Delta_F}{\eta_o}\right)^\alpha\right]\right\}^{\beta/\alpha} \quad (3)$$

where $\alpha = 2$, $\beta = D_f - 2$ as in fractal models (D_f: fractal dimension of the flame front), $\Delta_F = F \times \delta_L^0$ is the flame filter width, $\eta_o \approx 3L_t$ is the outer length scale (L_t: integral turbulent length scale, input for the model), η_i is the inner cut-off length-scale, related to the local Karlovitz number $\mathrm{Ka} = \tau_c/\tau_K$ (K: Kolmogorov scale)

$$\frac{\eta_i}{\delta_L^0} = \mathrm{Ka}^{-2} + r_1^* \mathrm{Ka}^{-1/2} \quad ; \quad r_1^* = (3C_q)^{3/4} \quad (4)$$

with $C_q = \frac{11}{3}C_u$, $C_u \approx 2$ being the "universal" constant in Kolmogorov's 2/3 law. The first term on the rhs of (4) accounts for low Karlovitz numbers, whereas the second one accounts for high Ka. The expression for β in (3) slightly differs from the one of Hawkes *et al.* (2012), and reads

$$3\beta = 1 + \frac{r_1^* \mathrm{Ka}^{-1/2}}{\mathrm{Ka}^{-2} + r_1^* \mathrm{Ka}^{-1/2}} \quad (5)$$

The main difficulty is to estimate the local Karlovitz number from the resolved field. Different expressions for Ka are

$$\mathrm{Ka} = \mathrm{Sc}\left(\frac{\delta}{\eta}\right)^2 = \mathrm{Sc}^{-1}\left(\frac{u_K}{S_L^0}\right)^2 = \frac{\sqrt{\varepsilon/\nu_u}}{S_L^0/\delta} \quad (6)$$

where δ is the diffusive thickness of the flame such that $\mathrm{Re}_f = \delta S_L^0/\nu_u = 1$, u_K is the Kolmogorov velocity scale, and $\mathrm{Sc} = \nu_u/D_{fuel\to air}$ is the Schmidt number usually assumed close to unity. The last expression for Ka in (6) can be used if a value is given to ε. This can be achieved from

$$\varepsilon = C_\varepsilon \frac{k_{sgs}^{3/2}}{\Delta} \approx C_\varepsilon \frac{u_\Delta^3}{\Delta} \quad ; \quad C_\varepsilon = 1.05 \quad (7)$$

where Δ and u_Δ are the (I)LES filter width and velocity fluctuation at scale Δ, respectively. One possibility is to compute ε from the subgrid scale eddy-viscosity given, e.g., by the Smagorinsky model, viz. $\varepsilon = \nu_{sgs}^{t\,3}/(C_s\Delta)^4$, with $C_s = 0.18$ and $\Delta \equiv h = (\Delta x \Delta y \Delta z)^{1/3}$. Colin *et al.* (2000) have proposed an operator called OP_2, based on the Laplacian of the curl of the resolved velocity field, to estimate u_Δ free from the thermal volumetric expansion across the flame front. These two approaches have been tested in this study.

NON-REACTING FLOW SIMULATIONS

Before going to the reacting CH_4/air flow, three ILES of the non-reacting air flow have been first performed, using the 5th order WENO-JS scheme. They are referred as NR#1, NR#2-1 and NR#2-2. In each case, the computational domain is a parallelepiped and the mesh is fully structured with clustering at the burner exit. Experimental data at 5 mm downstream the burner exit, for $P = 0.1$ MPa are (Fragner *et al.* (2015*b*)):

$k = 0.6125$ m^2/s^2 (turbulent kinetic energy)
$L_t = 4.25$ mm (integral scale, energetic eddies)
$\lambda = 1.25$ mm (Taylor micro-scale)
$\eta = 0.075$ mm (Kolmogorov scale)

The DNS resolution that matches these data corresponds to 330 grid points in the jet diameter. At this resolution, the numerical simulation of a computational domain of the size of the vessel shown in figure 2 is prohibitively expensive. Hence, a sharp Fourier cutoff (a low-pass filter) is applied to the spectral HIT velocity field, retaining about 90% of its kinetic energy, so that the filtered HIT injected at the inlet requires less grid points in the jet diameter.

In simulation NR#1, the full experimental domain is considered, and an idealized von Kàrmàn spectrum is applied. In simulation NR#2-1, a reduced domain is simulated with higher resolution, and the experimental spectrum of figure 4 is applied. Simulations NR#2-2 considers a slightly larger domain than NR#2-1, but the mesh is more clustered at the jet exit. Table 1 gathers the characteristics of these simulations.

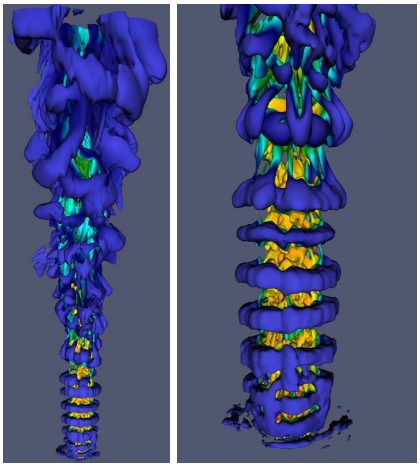

Figure 5. Simulation NR#1 (non-reacting). Q-criterion at $t = 0.8$ s, and zoom on the potential core.

Figure 5 shows the structure of the flow in simulation NR#1, using the Q-criterion iso-surface ($Q = 0.01$) colored by velocity magnitude. One can see, in the center, the injected turbulent field that evolves independently from the

Table 1. Parameters of the 3D non-reacting (NR), 2D and 3D reacting (R) simulations. The time step Δt is indicative.

	NR#1	NR#2-1	NR#2-2	R-2D#1	R-2D#2	R-3D
Forcing spectrum	von Kàrmàn	expe. (3D)	expe. (3D)	expe. (2D)	expe. (2D)	expe. (3D)
$L_x \times L_y \times L_z$ (m)	0.5×0.3×0.3	0.13×0.06×0.06	0.2×0.1×0.1	0.2×0.3×0	0.2×0.3×0	0.3×0.25×0.25
$N_x \times N_y \times N_z$	360×216×216	450×200×200	540×200×200	480×384×1	160×128×1	240×160×160
Total grid size	16.8×10^6	18.0×10^6	21.6×10^6	184320	20480	6.15×10^6
Points in jet ∅	56	100	100	107	36	50
$\Delta x_{min}/\eta$ - $/\delta_L^0$	6 -	3.3 -	3.3 -	3.1 - 0.47	9.3 - 1.4	6.7 - 1.0
α_{ASR} - CFL	10 - 0.8	10 - 0.8	10 - 0.8	1 - 0.4	1 - 0.4	1 - 0.8
Δt (s)	1.5×10^{-5}	0.8×10^{-5}	0.8×10^{-5}	0.54×10^{-7}	1.6×10^{-7}	1.5×10^{-6}

large scale Kelvin-Helmholtz structures arising from the inflectional instability of the jet. The zoom in figure 5 indicates a fast decay of the HIT (the Taylor micro-scale increases downstream) in the potential core (length ≈ 3 D). Further downstream, the breakdown to turbulence combines with the residual HIT to create a low-speed turbulent plume.

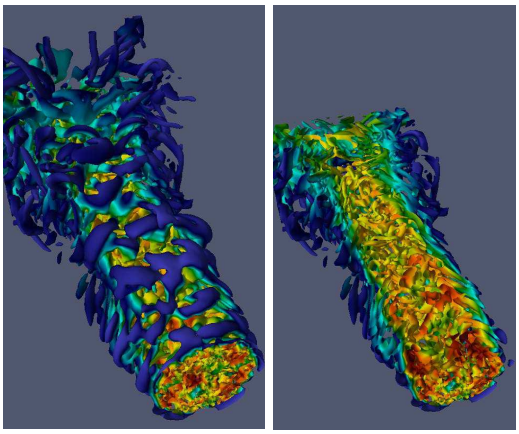

Figure 6. Simulation NR#2-1 (non-reacting). Q-criterion colored by velocity magnitude at $t = 0.14$ s near the injection (left), and detail of the inner structure of the jet (right).

Figure 6 is a visualization of the flow in simulation NR#2-1, in the injection region. Compared to NR#1, more detailed structures can be observed since the grid is refined. The evolution of kinetic energy on the jet axis in NR#2-1 and NR#2-2, is displayed in figure 7, in comparison with experimental data of Fragner *et al.* (2015*b*). Although the axial decay is faster than in the experiment, the length of the potential core, where production is negligible, is quite well predicted. The typical grid resolution of NR#2-1 or NR#2-2 (≈ 100 points in jet ∅) will be retained for 2D reacting flow simulations.

The CPU time for 0.8 s of physical time in simulation NR#1 is 36378 h on 108 Intel® Sandy Bridge® E5-4650 8-cores @2.70 GHz computational nodes (864 cores), corresponding to a wall-time of 42 h. The CPU time for 0.14 s (resp. 0.16) of physical time in simulation NR#2-1 (resp. NR#2-2) is 25200 h (resp. 31970) on 720 (resp. 864) cores (wall time 35 h (resp. 37)).

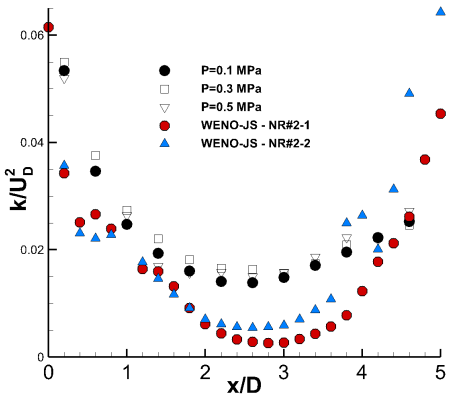

Figure 7. Simulations NR#2-1 and NR#2-2 (non-reacting). Turbulent kinetic energy along the jet axis.

REACTING FLOW SIMULATIONS

As a first step, the reacting air/CH_4 experiment at equivalence ratio $\phi = 0.8$ and $P = 0.1$ MPa is considered. The single step irreversible methane oxidation scheme given in Wang *et al.* (2011) is retained. At $\phi = 0.8$, the laminar flame velocity, the flame thermal thickness and the adiabatic burnt gas temperature are respectively $S_L^0 = 0.287$ m/s, $\delta_L^0 = 0.5$ mm and $T_b = 2015$ K. Further work will consider the skeletal Methane-air mechanism of Smooke & Giovangigli (1995) (16 species, 35 elementary reactions), before going to air/H_2/CO combustion using the 12 species (discarding Ar and He), 38 reversible reactions mechanism of Davis *et al.* (2005).

2D simulations: (I)LES strategy

For reasons of CPU cost, the different (I)LES strategies are first evaluated in 2D simulations, in a computational domain of size $L_x \times L_y = 0.2 \times 0.3$ m. The transverse size L_y has been increased, compared to NR#2-2, because the flame is flapping and interacts with side boundaries, leading to possible numerical instability. As a consequence, the mesh has been also modified. A fine grid, R-2D#1, has been built, which can almost resolve the flame front (2 points in δ_L^0) and serves as a reference. A coarse grid, R-2D#2, has also been generated by taking one point over three from grid R-2D#1. Their parameters are summarized in table 1. Sim-

ulations on mesh R-2D#1 have been performed with the 5th order WENO-OPT, MZ and JS schemes, sorted from the less to the most dissipative. Flame thickening F =1 (no thickening), 3, 6 and 12 have been applied, in association with the premixed combustion model, ε in (6) being computed from ν_{sgs}^t (but ν_{sgs}^t is not applied: ILES for flow dynamics). The case $F = 1$ with WENO-OPT leads to stable simulations on grid R-2D#1, so it is not far from a DNS due to the low dissipation of the scheme (subfilter resolution $r = \Delta/h = 15/13 \approx 1.1539$, Zhao *et al.* (2014)). It was however unstable on grid R-2D#2.

Figure 8 gathers instantaneous visualizations of the temperature progress variable. The first two rows correspond to R-2D#1, the third row to R-2D#2 and the last row to the experiment of Fragner *et al.* (2015*a*). The horizontal dashed line shows the experimental mean flame height, which is about 55 mm. In the first raw, the effect of flame thickening on the WENO-OPT simulations is apparent. The second row shows that it is corrected by the combustion model. The three cases F=1 (OPT, MZ and JS) produce similar flame lengths, close to the experiment.

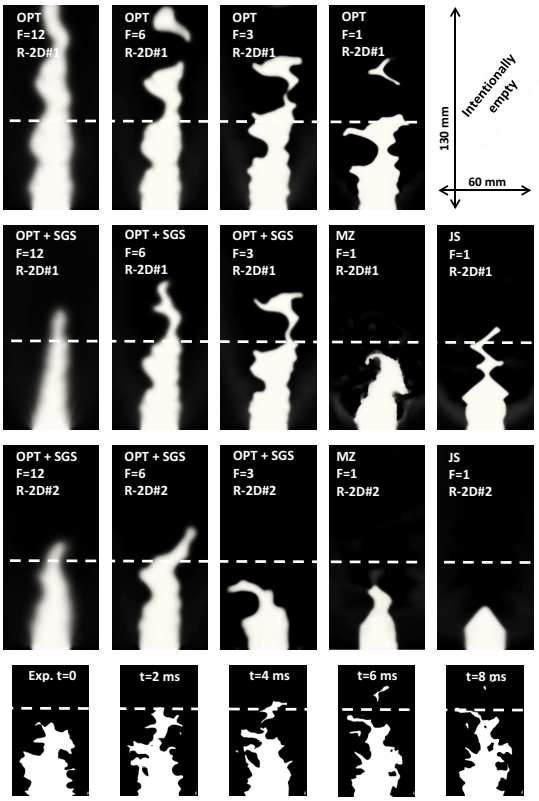

Figure 8. Progress variable for different 2D (I)LES strategies. Lower row: experimental flame front at 5 different times, $\phi = 0.8$, $P = 0.1MPa$.

Results on the coarse grid R-2D#2, displayed on the third row, show that large eddy simulations with the explicit sgs combustion model provide realistic flame lengths, whatever the thickening factor. ILES without any explicit modeling produces a too short flame, hence a too high S_T due to excessive numerical dissipation. This is particularly true for WENO-JS. However, WENO-MZ is not so far from the experiment.

3D simulations (work in progress)

The previous 2D simulations have shown that grid R-2D#2 is too coarse for ILES. On the other hand, grid R-2D#1 is too fine to be extended to 3D, for the available computational resources. Hence, an intermediate mesh R-3D has been built (see table 1). Calculations have been performed with WENO-OPT / $F = 6$, both without the sgs combustion model, and with the sgs model in which ε is computed either from OP_2 or from the Smagorinsky ν_{sgs}^t. This latter case produces a flame wrinkling $\Xi \approx 1$ therefore the model is almost inactive. The two left-most sub-figures in figure 9 show the (small) effect of the sgs model. The two right-most show that WENO-OPT / $F = 1$ is stable on the 3D grid, and that ILES produce a two short flame on this grid (≈ 1 point in δ_L^0).

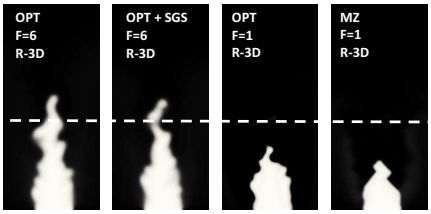

Figure 9. Progress variable for different 3D (I)LES strategies. Slice in the symmetry plane. The sgs model (2nd subfigure from the left) is computed with operator OP_2.

Figures 10 and 11 show the structure of the flow for the "best" WENO-OPT / $F = 6$ with sgs (OP_2), and the "worst" WENO-MZ / $F = 1$, cases respectively, at the same scale. The decay of injected turbulence is visibly faster for the more dissipative WENO-MZ than for WENO-OPT. It has also been observed in these simulations that for WENO-OPT / $F = 6$ with sgs, the (thickened) flame is distorted by turbulence but is stable, i.e. it stays at the same average location. For WENO-MZ / $F = 1$ on the other hand, the shape of the flame does not change much in time but the flame is flapping. This may generate the small-scale structures observed in the free shear layer of the burnt gas jet.

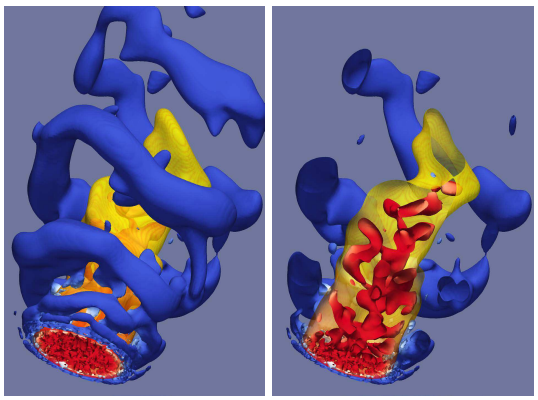

Figure 10. WENO-OPT / $F = 6$ + sgs (OP_2). Q-criterion colored by Y_{CH_4} (left), and inner structure of the flow (right). The flame surface is materialized by the $c = 0.5$ iso-surface (mainly yellow), colored by the reaction rate $\dot{\omega}_{CH_4}$.

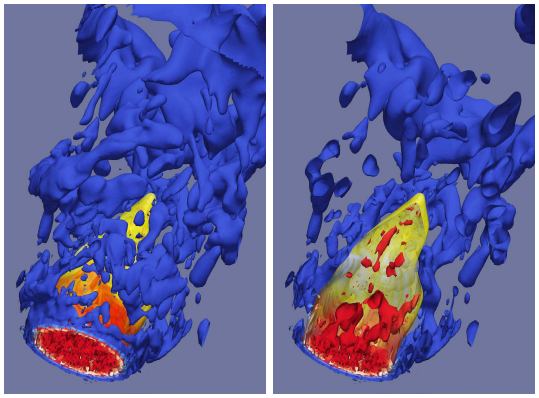

Figure 11. Same as figure 10, WENO-MZ, $F = 1$ (ILES).

CONCLUSION

This study has shown that the numerical dissipation of higher-order shock-capturing methods can lead to stable and realistic implicit large eddy simulations of turbulent premixed combustion on relatively coarse grids. The grid spacing must be about one laminar flame thickness to avoid excessive smearing of the diffusion layer. Under-resolution produces a too high flame speed, hence a too short flame length. However, explicit modeling associated with a low dissipation scheme leads to better results, in accordance with experimental data. Work is still needed to understand the intricate interactions between numerics, flow turbulence and flame wrinkling.

ACKNOWLEDGEMENTS

This work was granted access to the HPC resources of IDRIS under the allocations 2014-2b0913 and 2015-2b0913 made by GENCI (Grand Equipement National de Calcul Intensif). Song Zhao's fellowship is provided by the French Government's Investissement d'Avenir program: Laboratoire d'Excellence CAPRYSSES (Grant No ANR-11-LABX-0006-01).

REFERENCES

Borges, R., Carmona, M., Costa, B. & Don, W.S. 2008 An improved weighted essentially non-oscillatory scheme for hyperbolic conservation laws. *Journal of Computational Physics* **227**, 3191–3211.

Burcat, A. & Ruscic, B. 2006 On line database. Http://garfield.chem.elte.hu/Burcat/burcat.html.

Charlette, F., Meneveau, C. & Veynante, D. 2002 A power-law flame wrinkling model for LES of premixed turbulent combustion. Part I. *Combustion and Flame* **131**, 159–180.

Colin, O., Ducros, F., Veynante, D. & Poinsot, T. 2000 A thickened flame model for large eddy simulations of turbulent premixed combustion. *Physics of Fluids* **12** (7), 1668–1693.

Davis, S.G., Joshi, A.V., Wang, H. & Egolfopoulos, F. 2005 An optimized kinetic model of H_2/CO combustion. *Proceedings of the Combustion Institute* **30**, 1283–1292.

Ern, A. & Giovangigli, V. 1996 EGLIB: a general-purpose FORTRAN library for multicomponent transport property evaluation. CERMICS Internal Report, 96-51. http://blanche.polytechnique.fr/www.eglib/.

Fedioun, I., Lardjane, N. & Gökalp, I. 2001 Revisiting numerical errors in direct and large-eddy simulations of turbulence: Physical and spectral spaces analysis. *Journal of Computational Physics* **174**, 816–851.

Fragner, R., Halter, F., Mazellier, N., Chauveau, C. & Gökalp, I. 2015*a* Investigation of pressure effects on the small scale wrinkling of turbulent premixed bunsen flames. *Proceedings of the Combustion Institute* **35** (2), 1527–1535.

Fragner, R., Mazellier, N., Halter, F., Chauveau, C. & Gökalp, I. 2015*b* Multi-scale high intensity turbulence generator applied to a high pressure turbulent burner. *Flow, Turbulence and Combustion* **94** (1), 263–283.

Hawkes, E.R., Chatakonda, O., Kolla, H., Kerstein, A.R. & Chen, J.H. 2012 A petascale direct numerical simulation study of the modelling of flame wrinkling for large-eddy simulations in intense turbulence. *Combustion and flame* **159**, 2690–2703.

Henrick, A.K., Aslam, T.D. & Powers, J.M. 2005 Mapped weighted essentially non-oscillatory schemes: Achieving optimal order near critical points. *Journal of Computational Physics* **207**, 542–567.

Hinze, J.O. 1975 *Turbulence, 2nd edition*. Mc Graw Hill.

Jiang, G.S. & Shu, C.W. 1996 Efficient implementation of weighted ENO schemes. *Journal of Computational Physics* **126**, 202–228.

Karaca, M., Lardjane, N. & Fedioun, I. 2012 Implicit large eddy simulation of high-speed non-reacting and reacting air/h2 jets with a 5th order weno scheme. *Computers & Fluids* **62**, 25–44.

Mazellier, N., Danaila, B. & Renou, B. 2010 Multi-scale injection: a new tool to generate intense homogeneous and isotropic turbulence for premixed combustion. *Journal of Turbulence* **11** (43), 1–30.

Smooke, M. & Giovangigli, V. 1995 *Simplified transport and reduced chemistry models of premixed and non-premixed combustion. Modeling in Combustion Science* . Springer, Berlin/Heidelberg.

Thiesset, F., Maurice, G., Halter, F., Mazellier, N., Chauveau, C. & Gökalp, I. 2015 Modelling of the subgrid scale wrinkling factor for large-eddy simulation of turbulent premixed combustion. In *15th International Conference on Numerical Combustion*. Avignon, France, 19-22 April 2015.

Thompson, K.W. 1990 Time dependant boundary conditions for hyperbolic systems ii. *Journal of Computational Physics* **89**, 439–461.

Wang, G., Boileau, M. & Veynante, D. 2011 Implementation of a dynamic thickened flame model for large eddy simulations of turbulent premixed combustion. *Combustion and Flame* **158**, 2199–2213.

Wang, Y. & Trouvé, A. 2004 Artificial Acoustic Stiffness Reduction in Fully Compressible, Direct Numerical Simulation of Combustion. *Combustion Theory and Modelling* **8** (3), 633–660.

Yuen, F.T.C. & Gülder, Ö.L. 2013 Turbulent premixed flame front dynamics and implications for limits of flamelet hypothesis. *Proceedings of the Combustion Institute* **34**, 1393–1400.

Zhao, S., Lardjane, N. & Fedioun, I. 2014 Comparison of improved finite-difference WENO schemes for the implicit large eddy simulation of turbulent non-reacting and reacting high-speed shear flows. *Computers and Fluids* **95**, 74–87.